npj | Computational Materials

www.nature.com/npjcompumats

ARTICLE OPEN

Predicting Dirac semimetals based on sodium ternary compounds

Bo Peng[1,2], Changming Yue[1,3], Hao Zhang[2], Zhong Fang[1,4] and Hongming Weng[1,4,5]

Predicting new Dirac semimetals, as well as other topological materials, is challenging since the relationship between crystal structure, atoms and band topology is complex and elusive. Here, we demonstrate an approach to design Dirac semimetals via exploring chemical degree of freedom. Based on understanding of the well-known Dirac semimetal, Na_3Bi, three compounds in one family, namely Na_2MgSn, Na_2MgPb, and Na_2CdSn, are located. Furthermore, hybrid-functional calculations with improved accuracy for estimation of band inversion show that Na_2MgPb and Na_2CdSn have the band topology of Dirac semimetals. The nontrivial surface states with Fermi arcs on the (100) and (010) surfaces are shown to connect the projection of bulk Dirac nodes. Most importantly, the candidate compounds are dynamically stable and have been experimentally synthesized. The ideas in this work could stimulate further predictions of topological materials based on understanding of existing ones.

npj Computational Materials (2018)4:68 ; doi:10.1038/s41524-018-0124-5

INTRODUCTION

Dirac semimetals (DSMs)[1–5] are the three-dimensional (3D) analogs of graphene[6] with and only with Dirac nodes on the Fermi level. These Dirac nodes are formed by band crossing, and the low-energy excitation around them leads to quasiparticles described by Dirac equation as emergent massless Dirac fermions.[5,7–11] Up to now, there have been three classes of DSM proposed. One is the Dirac nodes with fourfold essential degeneracy, which is enforced by the nonsymmorphic symmetry at the high-symmetric momenta on the boundary of the Brillouin zone.[1] The second is the accidental degenerate Dirac nodes, which appears as the topological phase transition critical point between different topological insulating states.[12] The third one is also an accidental DSM, but the band crossing points are caused by band inversion and protected by proper crystal symmetry.[2,11] DSMs serve as a singular point of various topological states, such as topological insulators, Weyl semimetals, nodal line semimetals, and triple-point semimetals.[13] DSMs exhibit many novel properties, such as high carrier mobility,[14] unique surface states with Fermi arcs,[2,15] and negative longitudinal magnetoresistivity due to the chiral anomaly.[16,17]

The breakthrough in the search for stable DSMs[11] is achieved in the series of studies on Na_3Bi[2,4] and Cd_3As_2,[3,18–21] both of which were first proposed through first-principles calculations. They present good examples of the realization of the DSM in the above third class. The Dirac nodes are induced by band inversion and protected by proper axial rotational symmetry.[2,11] Such protection makes the Dirac nodes quite robust within a finite range of Hamiltonian parameters, which is exactly the reason why this class of DSM is experimentally available while the other two remain to be found.

Despite the success in identifying Na_3Bi and Cd_3As_2 and the intensive studies on them, to identify more DSMs remains a big challenge. How to locate a specific material among thousands of known compounds is not clear. Here, we demonstrate a chemically intuitive approach for searching new DSMs to show the underlying physics and ideas. We choose the first DSM Na_3Bi as a model system for tuning the chemical degree of freedom. Three sodium ternary compounds, Na_2MgSn, Na_2MgPb, and Na_2CdSn, are naturally selected. Further theoretical calculations reveal that the chemical trend in the elements of the same column in periodic table plays an important role in band inversion. The proposed general design principle can be used for finding new DSMs, as well as other topological materials.

RESULTS AND DISCUSSION

Material design

The crystal structure of Na_3Bi[2,7] can be viewed as the AB stacking of honeycomb layers along the *c*-axis, as shown in Fig. 1(a). For each honeycomb layer, one Na(1) atom and one Bi atom take the A and B sub-lattice site, respectively. There are two additional Na (2) atoms above and below the Na(1)-Bi honeycomb layer to connect the Bi atoms in the neighboring layers. As a well-understood DSM, its low-energy electronic band structure has been found to be mostly determined by the Na(1) and Bi atoms in the honeycomb layer. The two crossing bands along the Γ-A direction forming Dirac nodes are dominated by Na(1)-*s* orbitals and Bi $6p_{x,y}$ orbitals.[2] At Γ point the Na(1)-*s* bands are lower than those of Bi $6p_{x,y}$ mainly due to two things. One is that the heavy Bi has a relatively high on-site energy for 6*p* orbitals. The other is the interlayer coupling leads to splittings between the bonding and

[1]Beijing National Laboratory for Condensed Matter Physics, and Institute of Physics, Chinese Academy of Sciences, Beijing 100190, China; [2]Department of Optical Science and Engineering and Key Laboratory of Micro and Nano Photonic Structures (Ministry of Education), Fudan University, Shanghai 200433, China; [3]University of Chinese Academy of Sciences, Beijing 100049, China; [4]Collaborative Innovation Center of Quantum Matter, Beijing, China and [5]Songshan Lake Materials Laboratory, Dongguan, Guangdong 523808, China

Correspondence: Hao Zhang (zhangh@fudan.edu.cn) or Hongming Weng (hmweng@iphy.ac.cn)

These authors contributed equally: Bo Peng, Changming Yue

Received: 4 July 2018 Accepted: 6 November 2018
Published online: 04 December 2018

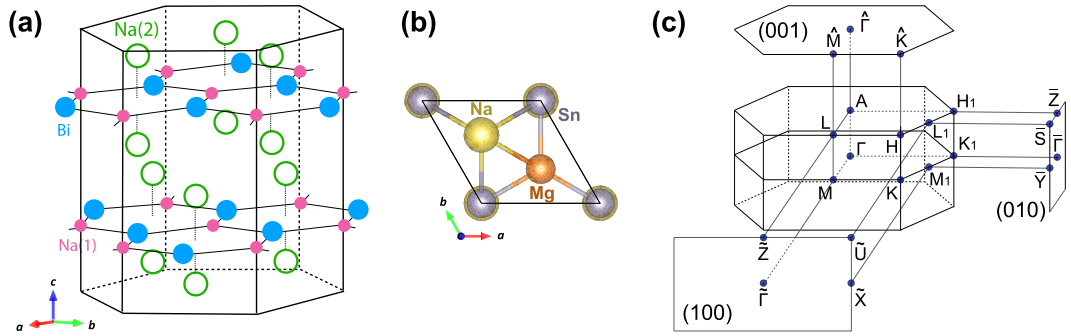

Fig. 1 **a** Crystal structure of Na_3Bi with Na(1), Na(2), and Bi sites indicated. **b** Top view of the Na_2MgSn unit-cell with Mg and Sn replacing Na(1) and Bi atoms in **a**, respectively. **c** The bulk Brillouin zone and the projected surface Brillouin zone for (100), (010), and (001) surfaces

Table 1. Optimized lattice constants, and lengths of the two shortest bonds (in-plane Mg/Cd-Sn/Pb bonds and vertical Na-Sn/Pb bonds) for Na_2MgSn, Na_2MgPb, and Na_2CdSn

	a (Å)	c (Å)	$d_{II\text{-}IV}$ (Å)	$d_{Na\text{-}IV}$ (Å)
Na_2MgSn	5.078 (5.049[29])	10.112 (10.095[29])	2.932 (2.915[29])	3.336 (3.328[29])
Na_2MgPb	5.157 (5.110[30])	10.240 (10.171[30])	2.977 (2.950[30])	3.375 (3.377[30])
Na_2CdSn	5.068 (4.990[31])	10.152 (10.111[31])	2.926	3.366

The experimental data are presented in parentheses for comparison

anti-bonding states for both *s* and *p* bands along Γ-A. These two crossing bands with different orbital characters have different irreducible representations along the Γ-A direction and the Dirac nodes are protected.

Inspired by the above understanding, we notice that Na_3Bi can be regarded as Na_2Na_1Bi. The first two Na are on Na(2) site, which support the 3D lattice structure and also supply two electrons to the Na(1)-Bi honeycomb layer. If the crystal structure and the electronic structure are similar to those of Na3Bi, one can get a new DSM material. Thus, this leads to the idea to find other potential DSMs by simply changing the atoms in the Na(1)-Bi layer. To induce band inversion, Bi should be substituted with other similar heavy metal atoms such as Pb and Sn. Since Pb and Sn have one fewer valence electron than Bi, to maintain the same band-filling, Na(1) should be substituted with atoms having two-valence electrons, such as alkaline-earth metal and II-B elements like Mg, Ca, Sr, Zn, Cd, and Hg. Thus, three sodium-containing ternary compounds reported experimentally, namely Na_2MgSn, Na_2MgPb, and Na_2CdSn, are naturally and immediately located. Na_2MgSn and Na_2MgPb have been successfully synthesized recently,[22,23] while Na_2CdSn has been synthesized and investigated in 1980.[24]

Similar to Na_3Bi, all these compounds crystallize in hexagonal lattice with the space group $P6_3/mmc$ (#194, D^4_{6h}). We take Na_2MgSn as an example, as demonstrated in Fig. 1(b). There are four Na atoms, two Mg atoms, and two Sn atoms in each unit-cell. The shortest bonds are those in the Mg-Sn layer. Na and Sn atoms align along the *c*-axis connected by the second shortest bonds. The optimized lattice constants and bond lengths are listed in Table 1, which are in good agreements with previous experimental results.[22–24]

For future experimental explorations, the stability of these three structures is an important aspect.[25–27] A material is dynamically stable when there is no imaginary phonon frequency existing in its phonon spectrum. As shown in Fig. 2, no imaginary phonon frequency is found in all three materials, indicating their dynamical stability at 0 K. This is consistent with the existence of them reported by experiments. As possible candidates for DSMs, one main advantage of these sodium ternary compounds compared to Na_3Bi is structural dynamic stability. For Na_3Bi, the $P6_3/mmc$ phase has been found dynamically unstable at the ground state due to large imaginary phonon frequencies.[28] In fact, even now the ground state of Na_3Bi is still under debate.[29,30]

Electronic structures

The calculated electronic structures of all three materials using the Perdew-Burke-Ernzerhof (PBE) functional and the Heyd-Scuseria-Ernzerhof (HSE) hybrid-functional are shown in the top and middle panels of Fig. 3, respectively. The fatted bands with the weight of projected atomic orbitals are also shown in the middle panel for each of them. We focus on the band structures along Γ-A, where the band inversion and Dirac nodes happen in Na_3Bi.

In general, the strength of band inversion between the bands composed of *s* orbitals (of Mg or Cd on Na(1) site) and *p* orbitals (of Sn or Pb on Bi site) follows the order of total atomic number (mass) of the atoms in the unit-cell within both PBE and HSE calculations. The overestimation of band inversion in PBE is improved by HSE calculation. One can find that the lightest Na_2MgSn has no band inversion and it is a normal semiconductor in HSE case. Na_2MgPb has the same total mass as Na_3Bi and is slightly lighter than the heaviest Na_2CdSn, but all of them have the similar band inversion along Γ-A.

The spin-orbit coupling (SOC) is further included and the band structures of them are shown in the bottom panel in Fig. 3. Both Na_2MgPb and Na_2CdSn are DSMs with Dirac nodes on the path Γ-A, while Na_2MgSn is an indirect band gap of 0.13 eV. For Na_2MgPb and Na_2CdSn, one notable difference from Na_3Bi is that there are two pairs of Dirac nodes since the one *s*-orbital band inverts with both the bonding and anti-bonding $p_{x,y}$-orbital bands. The *s*-band belongs to Γ_7 representation while the two $p_{x,y}$ bands belong to Γ_9 representation. The splitting in the bonding and anti-bonding $p_{x,y}$ (in-plane orbitals) bands along Γ-A (*z*-direction) seems quite small, indicating the weak interlayer coupling among these in-plane orbitals along the stacking direction.

Surface states

Similar to Na_3Bi, there will be surface states for DSMs Na_2MgPb and Na_2CdSn. To simulate surface states to be observed by the angle-resolved photoemission spectroscopy (ARPES), we use an iterative surface Green's function method,[31,32] where the HSE + SOC band structures are used in generating the maximally localized Wannier functions. The Brillouin zone of bulk and the projected surface Brillouin zones of (100), (010), and (001) planes are exactly the same as those of Na_3Bi,[2] WC-type ZrTe,[33] and KHgAs.[34] The projected surface density of states for the (100),

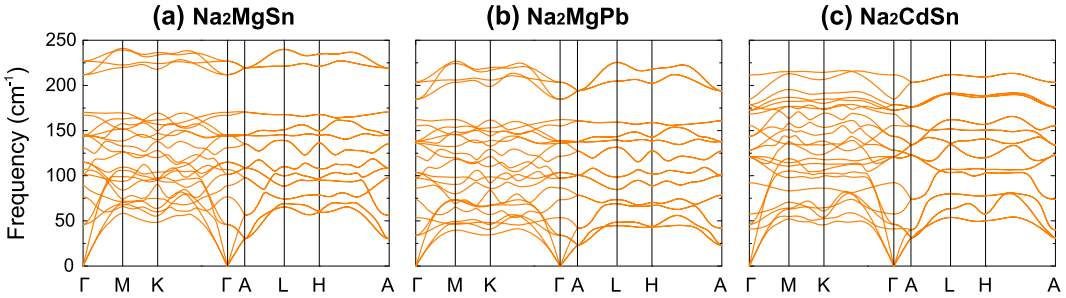

Fig. 2 Phonon dispersion for **a** Na_2MgSn, **b** Na_2MgPb, and **c** Na_2CdSn

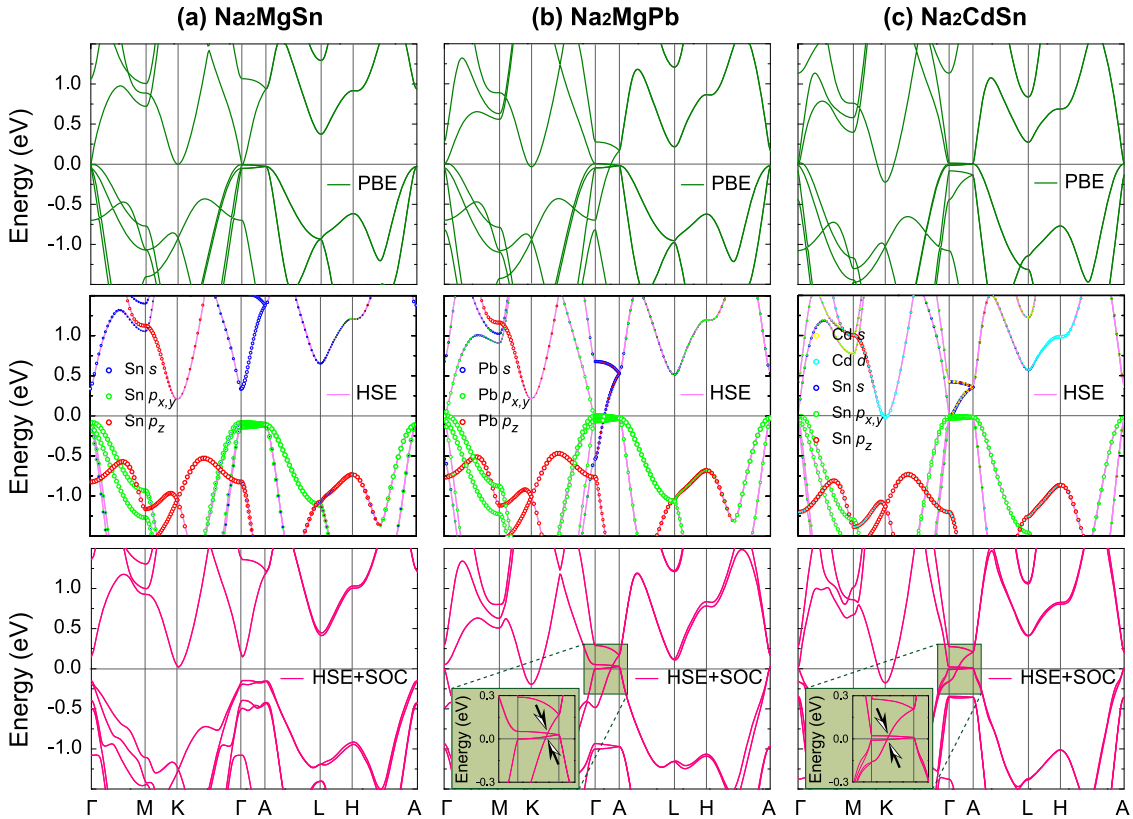

Fig. 3 Calculated electronic structures for **a** Na_2MgSn, **b** Na_2MgPb, and **c** Na_2CdSn using the PBE functional without spin-orbit coupling (top panel), and hybrid-functional without (middle panel) and with (bottom panel) spin-orbit coupling. The fatted bands with the weight of atomic orbital projection near the Fermi level are present in the middle panel. The two arrows point out the two Dirac cones formed by band crossings from *s*-band and bonding, anti-bonding $p_{x,y}$ – bands along Γ-A

(010), and (001) surfaces of Na_2MgPb are shown in Fig. 4(a)–(c). On both (100) and (010) side surfaces, the projection of bulk Dirac cone (pointed by the arrow) is well separated from the topological surface Dirac cone (labeled by the circle). The surface Dirac cone has its branches merging into the bulk states at the projection of 3D Dirac point, which leads to the arc like Fermi surface when the Fermi level is set at the bulk Dirac nodal point. There are two Fermi arcs touch each other at the surface projection of bulk Dirac point at 61 meV, as shown in Fig. 4(d, e). For the (001) surface, the projection of bulk Dirac nodes overlaps with the surface Dirac cone as shown in Fig. 4(c), which is similar to the case in Na_3Bi.[2,4]

The projected surface density of states for the (100), (010), and (001) surfaces of Na_2CdSn are shown in Fig. 5. For both the (100) and (010) surfaces, the bulk Dirac cone is closer to the Γ point. Due to the smaller band splitting between the bonding and anti-bonding $p_{x,y}$ – orbital bands, the nontrivial surface states of Na_2CdSn are not as clear as those in Na_2MgPb. For the (100) surface, the Fermi arcs are hidden within the projection of the bulk states on the surface. They can be well revealed in the Fermi surface plot on the (010) surface with Fermi level at bulk Dirac point of 40 meV, as shown in Fig. 5(e). For the (001) surface, the surface projection of the bulk states is superposed with the nontrivial surface states, which is similar to the case in Na_2MgPb.

In this paper, we demonstrate an approach for searching new DSM materials by tuning the chemical degree of freedom based on material design of well-known DSM Na_3Bi. By keeping both the crystal and electronic structures essentially identical to Na_3Bi, three compounds Na_2MgSn, Na_2MgPb, and Na_2CdSn are naturally located and two of them are identified as DSM candidates based on our theoretical calculations. The phonon calculations confirm that these compounds are stable than Na_3Bi, paving the way for experimental verification. The hybrid-functional calculations with

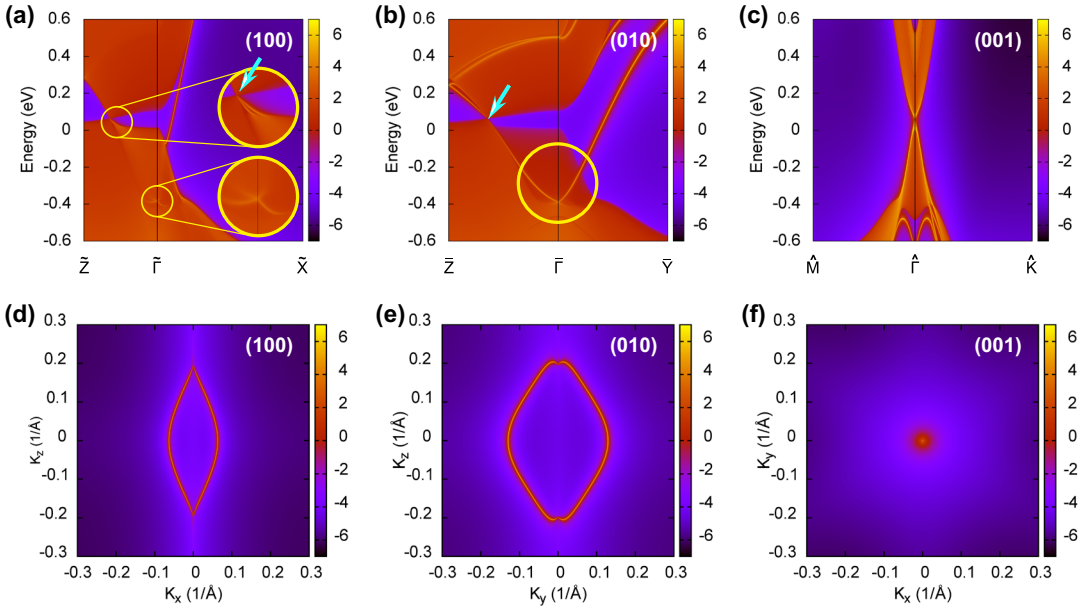

Fig. 4 Surface band structure for **a** (100), **b** (010), and **c** (001) surfaces of Na_2MgPb. The arrow points out the bulk Dirac cone, and the circle labels the topological surface states due to $Z_2 = 1$ in $k_z = 0$ plane. The corresponding Fermi surface with Fermi level at bulk Dirac point (61 meV) is shown in **d**–**f**

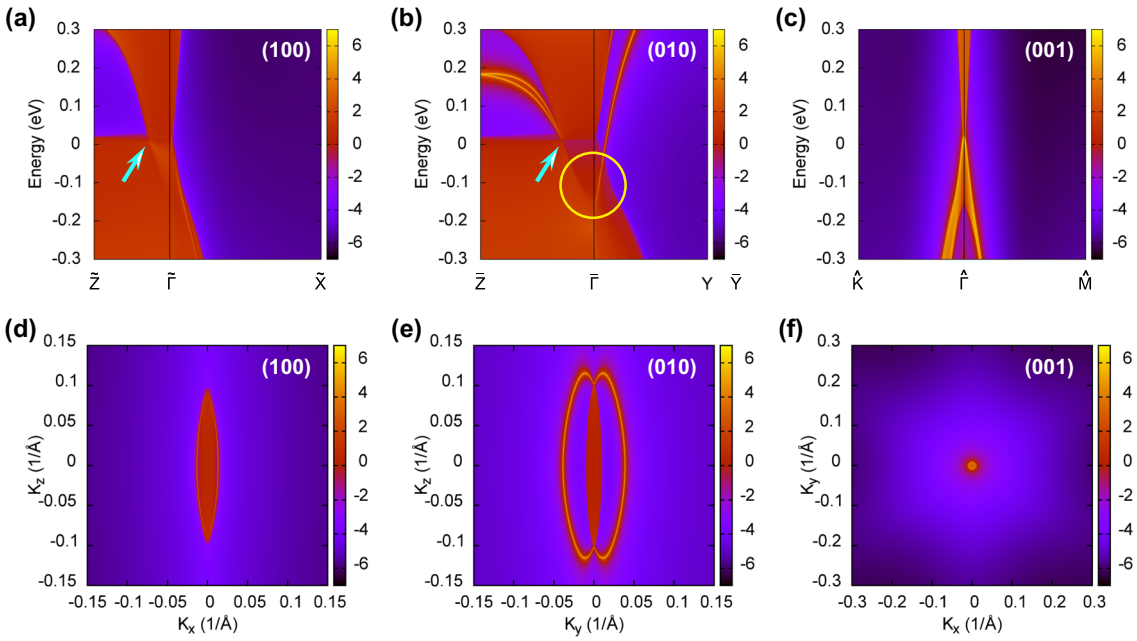

Fig. 5 Surface band structure for **a** (100), **b** (010), and **c** (001) surfaces of Na_2CdSn. The arrow points out the bulk Dirac cone, and the circle labels the topological surface states. The corresponding Fermi surface with Fermi level at bulk Dirac point (40 meV) is shown in **d**–**f**

spin-orbit coupling show that Na_2MgSn is an indirect band gap normal semiconductor. By substituting Sn by heavier Pb, the band inversion occurs, and the Dirac nodes due to band crossing are protected by crystal symmetry in Na_2MgPb. For Na_2CdSn, the band inversion is induced by replacing Mg with heavier Cd in Na_2MgSn. Moreover, the coexistence of both a bulk 3D Dirac cone and topological surface states can be observed in the projected surface density of states for side surfaces (100) and (010), which can be used as a reference for further experimental validation in ARPES or scanned tunneling microscopy measurements. We hope the idea in this example would lead to more material design efforts based on known topological materials for more successful and efficient predictions.

During the preparation of this manuscript, ref. [35] proposed that Na_2CdSn is a topological crystalline insulator (TCI) candidate, which is consistent with our PBE + SOC calculation. From Fig. 3(c), it is seen that both bonding and anti-bonding *s* bands are lower than the $p_{x,y}$ bands along the whole path Γ-A. And we have confirmed that in this case it is a TCI of $Z_{12} = 8$[36] with mirror Chern number 2 in m_{001} plane.

METHODS

First-principles calculations are performed using the Vienna ab-initio simulation package (VASP)[37] based on density functional theory (DFT). The generalized gradient approximation (GGA) in the PBE parameterization for the exchange-correlation functional is used for structural relaxation. A plane-wave basis set is employed with kinetic energy cutoff of 500 eV. We use the projector-augmented-wave method and the related pseudopotential for each element. A $11 \times 11 \times 5$ **q**-mesh is used during structural relaxation for the unit-cell until the energy difference is converged within 10^{-6} eV, with a Hellman-Feynman force convergence threshold of 10^{-4} eV/Å. To improve the underestimation of band gap in the PBE functional, hybrid-functional method based on the HSE method are adopted.[38–40] The harmonic interatomic force constants (IFCs) are obtained by density functional perturbation theory using a $3 \times 3 \times 2$ supercell with a $3 \times 3 \times 3$ **q**-mesh. The phonon dispersion is calculated from the harmonic IFCs using the PHONOPY code.[41,42] The Wannier functions[43] for Cd/Mg *s*-orbital and Sn/Pb *s*-and *p*-orbitals are generated, which are used in the surface state calculations.

DATA AVAILABILITY

The datasets generated during and/or analyzed during the current study are available from the corresponding author on reasonable request.

ACKNOWLEDGEMENTS

We thank the valuable discussions with X. Wan, C. Fang, Z. Song, and T. Zhang. This work is supported by the the National Key Research and Development Program of China (No. 2016YFA0300600 and 2018YFA0305700), the National Natural Science Foundation of China (Grant Nos. 11374063 and 11674369) and the "Strategic Priority Research Program (B)" of the Chinese Academy of Sciences (Grant No. XDB07020100).

AUTHOR CONTRIBUTIONS

H.M.W. and H.Z. designed the research. B.P., C.M.Y., and H.Z. performed the calculations. B.P., H.M.W., Z.F., and H.Z. analyzed and discussed the results. B.P. and W. H.M. wrote the text of the manuscript. B.P. and C.M.Y. contributed equally to this work. All authors commented on the manuscript.

ADDITIONAL INFORMATION

Competing Interests: The authors declare no competing interests.

Publisher's note: Springer Nature remains neutral with regard to jurisdictional claims in published maps and institutional affiliations.

REFERENCES

1. Young, S. M. et al. Dirac semimetal in three dimensions. *Phys. Rev. Lett.* **108**, 140405 (2012).
2. Wang, Z. et al. Dirac semimetal and topological phase transitions in A_3Bi (A = Na, K, Rb). *Phys. Rev. B* **85**, 195320 (2012).
3. Wang, Z., Weng, H., Wu, Q., Dai, Xi & Fang, Z. Three-dimensional Dirac semimetal and quantum transport in Cd_3As_2. *Phys. Rev. B* **88**, 125427 (2013).
4. Weng, H., Dai, Xi & Fang, Z. Topological semimetals predicted from first-principles calculations. *J. Phys.: Condens. Matter* **28**, 303001 (2016).
5. Armitage, N. P. et al. Weyl and Dirac semimetals in three-dimensional solids. *Rev. Mod. Phys.* **90**, 015001 (2018).
6. Novoselov, K. S. et al. Electric field effect in atomically thin carbon films. *Science* **306**, 666 (2004).
7. Liu, Z. K. et al. Discovery of a three-dimensional topological dirac semimetal, Na_3Bi. *Science* **343**, 864 (2014).
8. Bradlyn, B. et al. Beyond Dirac and Weyl fermions: Unconventional quasiparticles in conventional crystals. *Science* **353**, aaf5037 (2016).
9. Bernevig, A., Weng, H., Fang, Z. & Dai, Xi Recent progress in the study of topological semimetals. *J. Phys. Soc. Jpn.* **87**, 041001 (2018).
10. Orlita, M. et al. Observation of three-dimensional massless Kane fermions in a zinc-blende crystal. *Nat. Phys.* **10**, 233 (2014).
11. Yang, B. -J. & Nagaosa, N. Classification of stable three-dimensional Dirac semimetals with nontrivial topology. *Nat. Commun.* **5**, 4898 (2014).
12. Murakami, S. Phase transition between the quantum spin Hall and insulator phases in 3D: emergence of a topological gapless phase. *New J. Phys.* **9**, 356 (2007).
13. Weng, H. Fang, C., Fang, Z. & Dai, X. A new member in topological semimetals family. *Natl Sci. Rev.* **4**, 798–799 (2017).
14. Zdanowicz, W. & Zdanowicz, L. Semiconducting compounds of the AII BV group. *Annu. Rev. Mater. Sci.* **5**, 301–328 (1975).
15. Wan, X., Turner, A. M., Vishwanath, A. & Savrasov, S. Y. Topological semimetal and Fermi-arc surface states in the electronic structure of pyrochlore iridates. *Phys. Rev. B* **83**, 205101 (2011).
16. Xiong, J. et al. Evidence for the chiral anomaly in the Dirac semimetal Na_3Bi. *Science* **350**, 413 (2015).
17. Gorbar, E. V., Miransky, V. A. & Shovkovy, I. A. Chiral anomaly, dimensional reduction, and magnetoresistivity of Weyl and Dirac semimetals. *Phys. Rev. B* **89**, 085126 (2014).
18. Liu, Z. K. et al. A stable three-dimensional topological Dirac semimetal Cd_3As_2. *Nat. Mater.* **13**, 677–681 (2014).
19. Borisenko, S. et al. Experimental realization of a three-dimensional Dirac semimetal. *Phys. Rev. Lett.* **113**, 027603 (2014).
20. Jeon, S. et al. Landau quantization and quasiparticle interference in the three-dimensional Dirac-semimetal Cd_3As_2. *Nat. Mater.* **13**, 851–856 (2014).
21. Neupane, M. et al. Observation of a three-dimensional topological Dirac semimetal phase in high-mobility Cd_3As_2. *Nat. Commun.* **5**, 3786 (2014).
22. Yamada, T., Deringer, V. L., Dronskowski, R. & Yamane, H. Synthesis, crystal structure, chemical bonding, and physical properties of the ternary Na/Mg stannide Na_2MgSn. *Inorg. Chem.* **51**, 4810–4816 (2012).
23. Yamada, T. et al. Synthesis, crystal structure, and high-temperature phase transition of the novel plumbide Na_2MgPb. *Inorg. Chem.* **53**, 5253–5259 (2014).
24. Matthes, H. & Schuster, R. Ternary sodium phases with cadmium or mercury and tin or lead. *Z. für Naturforsch. B* **35**, 778–780 (1980).
25. Zhang, R. F. et al. Stability and strength of transition-metal tetraborides and triborides. *Phys. Rev. Lett.* **108**, 255502 (2012).
26. Zhou, L. et al. Structural stability and thermodynamics of CrN magnetic phases from ab initio calculations and experiment. *Phys. Rev. B* **90**, 184102 (2014).
27. Peng, Bo et al. Stability and strength of atomically thin borophene from first principles calculations. *Mater. Res. Lett.* **5**, 399–407 (2017).
28. Cheng, X. et al. Ground-state phase in the three-dimensional topological Dirac semimetal Na_3Bi. *Phys. Rev. B* **89**, 245201 (2014).
29. Cheng, X., Li, R., Li, D., Li, Y. & Chen, X. -Q. Stable compositions and structures in the Na-Bi system. *Phys. Chem. Chem. Phys.* **17**, 6933–6947 (2015).
30. Shao, D. et al. Strain-induced quantum topological phase transitions in na_3Bi. *Phys. Rev. B* **96**, 075112 (2017).
31. Zhang, W., Yu, R., Zhang, H. -J., Dai, Xi & Fang, Z. First-principles studies of the three-dimensional strong topological insulators Bi_2Te_3, Bi_2Se_3 and Sb_2Te_3. *New J. Phys.* **12**, 065013 (2010).
32. Wu, QuanSheng, Zhang, ShengNan, Song, H. -F., Troyer, M. & Soluyanov, A. A. WannierTools: An open-source software package for novel topological materials. *Comput. Phys. Commun.* **224**, 405–416 (2018).
33. Weng, H., Fang, C., Fang, Z. & Dai, Xi Coexistence of weyl fermion and massless triply degenerate nodal points. *Phys. Rev. B* **94**, 165201 (2016).
34. Wang, Z., Alexandradinata, A., Cava, R. J. & Bernevig, B. A. Hourglass fermions. *Nature* **532**, 189– (2016).
35. Tang, F., Po, H. C., Vishwanath, A. & Wan, X. Topological materials discovery by largeorder symmetry indicators, arXiv 1806, 04128 (2018).
36. Song, Z., Zhang, T., Fang, Z. & Fang, C. Quantitative mappings between symmetry and topology in solids. *Nat. Commun.* **9**, 3530 (2018).
37. Kresse, G. & Furthmüller, J. Efficient iterative schemes for ab initio total-energy calculations using a plane-wave basis set. *Phys. Rev. B* **54**, 11169–11186 (1996).
38. Heyd, J., Scuseria, G. E. & Ernzerhof, M. Hybrid functionals based on a screened Coulomb potential. *J. Chem. Phys.* **118**, 8207 (2003).
39. Heyd, J., Scuseria, G. E. & Ernzerhof, M. Erratum: ybrid functionals based on a screened Coulomb potential?. *J. Chem. Phys.* **124**, 219906 (2006).
40. Peralta, J. E., Heyd, J., Scuseria, G. E. & Martin, R. L. Spin-orbit splittings and energy band gaps calculated with the Heyd-Scuseria-Ernzerhof screened hybrid functional. *Phys. Rev. B* **74**, 073101 (2006).
41. Togo, A., Oba, F. & Tanaka, I. First-principles calculations of the ferroelastic transition between rutile-type and $CaCl_2$-type SiO_2 at high pressures. *Phys. Rev. B* **78**, 134106 (2008).
42. Togo, A. & Tanaka, I. First principles phonon calculations in materials science. *Scr. Mater.* **108**, 1–5 (2015).
43. Mostofi, A. A. et al. An updated version of Wannier90: A tool for obtaining maximallylocalised Wannier functions. *Comput. Phys. Commun.* **185**, 2309–2310 (2014).